DNA double-strand breaks in cancer cells as a function of proton linear energy transfer and its variation in time

Otilija Keta, Vladana Petković, Pablo Cirrone, Giada Petringa, Giacomo Cuttone, Dousatsu Sakata, Wook-Geun Shin, Sebastien Incerti, Ivan Petrović, Aleksandra Ristić Fira

DNA double-strand breaks in cancer cells as a function of proton linear energy transfer and its variation in time

Otilija Keta
,
Vladana Petković
,
Pablo Cirrone
,
Giada Petringa
,
Giacomo Cuttone
,
Dousatsu Sakata
,
Wook-Geun Shin
,
Sebastien Incerti
,
Ivan Petrović
&
Aleksandra Ristić Fira
show less

Received 24 Mar 2021, Accepted 21 Jun 2021, Accepted author version posted online: 30 Jun 2021, Published online: 19 Jul 2021

- Download citation

- https://doi.org/10.1080/09553002.2021.1948140

- CrossMark

In this article

- Abstract
- Introduction
- Materials and methods
- Results
- Discussion
- Conclusion
- Disclosure statement
- Additional information
- References

Abstract

Purpose

The complex relationship between linear energy transfer (LET) and cellular response to radiation is not yet fully elucidated. To better characterize DNA damage after irradiations with therapeutic protons, we monitored formation and disappearance of DNA double-strand breaks (DNA DSB) as a function of LET and time. Comparisons with conventional γ-rays and high LET carbon ions were also performed.

Materials and Methods

In the present work, we performed immunofluorescence-based assay to determine the amount of DNA DSB induced by different LET values along the 62 MeV therapeutic proton Spread out Bragg peak (SOBP) in three cancer cell lines, i.e. HTB140 melanoma, MCF-7 breast adenocarcinoma and HTB177 non-small lung cancer cells. Time dependence of foci formation was followed as well. To determine irradiation positions, corresponding to the desired LET values, numerical simulations were carried

out using Geant4 toolkit. We compared γ-H2AX foci persistence after irradiations with protons to that of γ-rays and carbon ions.

Results

With the rise of LET values along the therapeutic proton SOBP, the increase of γ-H2AX foci number is detected in the three cell lines up to the distal end of the SOBP, while there is a decrease on its distal fall-off part. With the prolonged incubation time, the number of foci gradually drops tending to attain the residual level. For the maximum number of DNA DSB, irradiation with protons attain higher level than that of γ-rays. Carbon ions produce more DNA DSB than protons but not substantially. The number of residual foci produced by γ-rays is significantly lower than that of protons and particularly carbon ions. Carbon ions do not produce considerably higher number of foci than protons, as it could be expected due to their physical properties.

Conclusions

In situ visualization of γ-H2AX foci reveal creation of more lesions in the three cell lines by clinically relevant proton SOBP than γ-rays. The lack of significant differences in the number of γ-H2AX foci between the proton and carbon ion-irradiated samples suggests an increased complexity of DNA lesions and slower repair kinetics after carbon ions compared to protons. For all three irradiation types, there is no major difference between the three cell lines shortly after irradiations, while later on, the formation of residual foci starts to express the inherent nature of tested cells, therefore increasing discrepancy between them.

Keywords:

Human malignant cellsγ-raysprotonscarbon ionsDNA double-strand breaks

Previous article**View** latest articles**Next** article

Introduction

Even though photons are still the most frequently used tool in radiotherapy, the therapeutic advantages of irradiations with ions have been increasingly recognized (Malouff et al. 2020). Due to their different physical characteristics, photon and ion beams, such as protons and carbon ions, differ in their energy transfer profiles. Protons and carbon ions display a specific, highly concentrated dose distribution in depth known as the Bragg peak which allows for radiation to be precisely delivered to the tumor. In addition, rather low levels of energy are deposited in tissues proximal and distal to the tumor, thus minimizing the damage to the adjacent, healthy tissue (Liu and Chang 2011; van de Water et al. 2011; Loeffler and Durante 2013; Vitti and Parsons 2019; Malouff et al. 2020). One of the main parameters which define the biological outcomes of ionizing radiation is the linear energy transfer (LET) (Tommasino and Durante 2015; Oeck et al. 2018). It is well recognized that high LET particles possess stronger cell

killing abilities than low LET radiation. In contrast to photons, ion irradiation is characterized by higher LET because it deposits high density of energy along the particle track, increasing toward the end of the range (Hagiwara et al. 2019).

The relative biological effectiveness (RBE), which represents the ratio of the biological effect between reference (photon) radiation and tested radiation, is considered in therapeutic practice to be slightly higher than unity for protons (Durante et al. 2017) but increases for heavier particles. Thus, carbon ions demonstrate 2 to 3, or even more, fold greater RBE than photons (Choi and Kang 2012). However, there is an increased concern that the fixed proton RBE value of 1.1 is an oversimplification because LET increases toward the end of the Bragg-peak which potentially exposes the neighboring healthy tissue to risk (Paganetti et al. 2002; Durante et al. 2017; Ilicic et al. 2018; Ray et al. 2018; Vitti and Parsons 2019). Higher RBE of particle radiation can be explained by greater complexity of induced DNA damage, which is more difficult for the cell to repair (Ostashevsky 1989; Goodhead et al. 1993; Goodhead 1994; Schipler and Iliakis 2013).

Currently, radiotherapy faces limited biological personalization. Even though the radiosensitivity of normal tissues as well as cancer cells varies considerably, the uniform radiation sensitivity over the entire population has been anticipated (Cooke et al. 2011; McMahon et al. 2017). Due to RBE dependence on physical and biological parameters and significant uncertainties resulting from complex RBE–LET relationship, biophysical models are important for the estimation of clinically relevant RBE values (Paganetti 2014, 2018; Mein et al. 2019). To make predictions about response of cells to irradiation, cell-specific data such as dose response information is needed, because RBE depends on the underlying intrinsic radiosensitivity of cells. By improving our basic knowledge about DNA damage repair, as it is the major determinant of cellular radiosensitivity, a better predictive capability with lower uncertainties can be obtained (McMahon et al. 2017). Nevertheless, the exact mechanisms that lie at the basis of radiation-induced single-strand breaks (SSB), double-strand breaks (DSB) and clustered/complex DNA lesions as well as the great variation of pathways that are involved in response to DNA damage have not yet been fully elucidated (Asaithamby et al. 2011; Chatzipapas et al. 2020; Nickoloff et al. 2020).

Initial concept for modeling radiation induced DNA damage originates back in the early 1990s (Nikjoo et al. 1994). Geant4-DNA has been developed to integrate mechanisms of DNA damage caused by ionizing radiation into open-source simulation platform (Incerti, Baldacchino, et al. 2010; Incerti, Ivanchenko, et al. 2010; Bernal et al. 2015; Incerti et al. 2018). It is fully included in the Geant4 Monte Carlo toolkit (Agostinelli et al. 2003; Allison et al. 2006, 2016) and can use continuous chromatin geometry to simulate early DNA damage and to calculate the SSB and DSB that arise from direct and indirect damage (Sakata et al. 2019, 2020). Often, for the detection and evaluation of DSB yields, immunofluorescent imaging of DNA repair markers such as γ-H2AX foci are used, even though the relation between foci yields and the number of DSB is proportional, but yet unclear (Ray et al. 2018; Sakata et al. 2020). Albeit a reasonable agreement between literature data and Geant4-DNA simulations has been found, there

is still a need to fully validate the models against experimental data (Incerti et al. 2013, 2016).

In the present work, we aimed to gain more insight into variations of DNA damage, through DSB formation, induced by therapeutic protons. Followed alterations are examined as a function of LET and time. For this purpose, human radioresistant cancer cells of different origins, that is, HTB140 melanoma, MCF-7 breast adenocarcinoma and HTB177 non-small lung cancer cells are used. Irradiation of cell samples is performed along the 62 MeV therapeutic proton spread out Bragg peak (SOBP), thus obtaining various LET values. For the one being in the middle of the SOBP, the time course of γ-H2AX foci formation and degradation is followed. To better position the results of DNA damage that arises after exposure to proton irradiation, conventional γ-rays and carbon ions, as a high LET specie, are also included. The selection of cell lines regarding the size and shape of their nuclei, as well as the level of their radiosensitivity will be an important step toward the improvement and validation of the Geant4-DNA numerical simulation toolkit.

Materials and methods

Cell culture

Human HTB140 melanoma, MCF-7 breast adenocarcinoma and HTB177 non-small lung cancer cells that are used in this study, were purchased from ATCC (Rockville, MD, USA). Cells were cultured in RPMI 1640 cell culture medium supplemented by 10% fetal bovine serum, penicillin/streptomycin and L-glutamine (Sigma-Aldrich Chemie GmbH, Steinheim, Germany) and kept in a humidified incubator (Heraeus, Hanau, Germany) at 37 °C and 5% CO2.

In the performed experiments, prior to irradiations, cell lines were seeded in slide flasks, in a suitable number to provide exponential growth of cells at the time of irradiation. Throughout irradiations, flasks were fully loaded with precooled culture medium (~4 °C), and positioned upright in a specific device to meet horizontal ion beams. Equal settings were maintained for the control samples as for those that were irradiated. In order to provide correct comparison of obtained data, in all experiments carried out either with γ-rays, protons or carbon ions, for each cell line, even experimental conditions were precisely followed.

Cell cycle analysis

Before irradiation the analysis of cell cycle distribution of cell lines was performed. Samples were trypsinized, centrifuged and washed with PBS. After fixation in 70% ice-cold ethanol, cells were washed in PBS and incubated with RNAse A (Serva Electrophoresis GmbH, Heidelberg, Germany) in PBS (1 mg/ml) for 20 min at 37 °C. DNA staining was performed by incubation with propidium iodide solution in PBS

(50 µg/ml) for 10 min at room temperature in the dark. Cell cycle analysis was performed on CyFlow® cytometer (Partec, GmbH, Münster, Germany) using FloMax® software. For each sample, 10 000 cells were analyzed.

Irradiation conditions

Irradiations with γ-rays issued by ^{60}Co source (CIRUS-Cis Biointernational, Gif-sur-Yvette, France) were performed at the Vinča Institute of Nuclear Sciences, Belgrade, Serbia. Cells were irradiated with the dose of 1 Gy at the rate of ∼1 Gy/min, in air at ∼4 °C since the inhibition of repair processes is required.

Proton and carbon ion irradiations are done using beams delivered by the superconducting cyclotron at the Instituto Nazionale di Fisica Nucleare (INFN), Laboratori Nazionali del Sud (LNS) in Catania in Italy. In all irradiations, cells were exposed to the dose of 1 Gy at the rate of ∼12 Gy/min, in air at ∼4 °C to minimize activation of repair processes. Samples are irradiated in four positions along the 62 MeV therapeutic proton SOBP of the CATANA (Centro di AdroTerapia e Applicazioni Nucleari Avanzate) facility for treatment of eye melanoma (Cirrone et al. 2017), thus providing different LET values. The chosen irradiation sites are achieved by placing Perspex (polymethyl methacrylate – PMMA) plates, having various thicknesses, in front of the samples. As shown in Table 1, the selected PMMA thicknesses are 4.6, 16.3, 23.8 and 24.6 mm, corresponding to 85.7, 99.8, 100.2 and 38.7% of relative dose, hence giving dose averaged LET (LET_{dose}) values of 2.2, 4.4, 11.3 and 19.3 keV/µm, respectively specifying irradiation positions A, B, C and D. Depth dose distribution in Perspex (PMMA) of the 62 MeV therapeutic proton SOBP is experimentally obtained using plane-parallel PTW 34045 Markus ionizing chamber (Advanced Markus Chamber, 0.02 cm^2, Type 34045, Physikalisch Technische Werkstatten – PTW, Freiberg, Germany) and is given in Figure 1 together with marked irradiation positions. The chamber is calibrated following the IAEA Technical Report Series (IAEA 2000) code of practice, while the precision of positioning is of ∼50 µm (Cirrone et al. 2004; Petrovic et al. 2010). To verify the precision of positioning of cell samples prior to each irradiation, GafChromic HS films (ISP Technologies, Wayne, NJ) are interposed.

Figure 1. Measured and simulated depth dose and depth LET_{dose} distribution in Perspex (PMMA) of the 62 MeV proton SOBP beam. Arrows indicate irradiation positions. The ordinate on the left side is related to experimental and simulated dose distributions, while the right one corresponds to dose averaged LET.

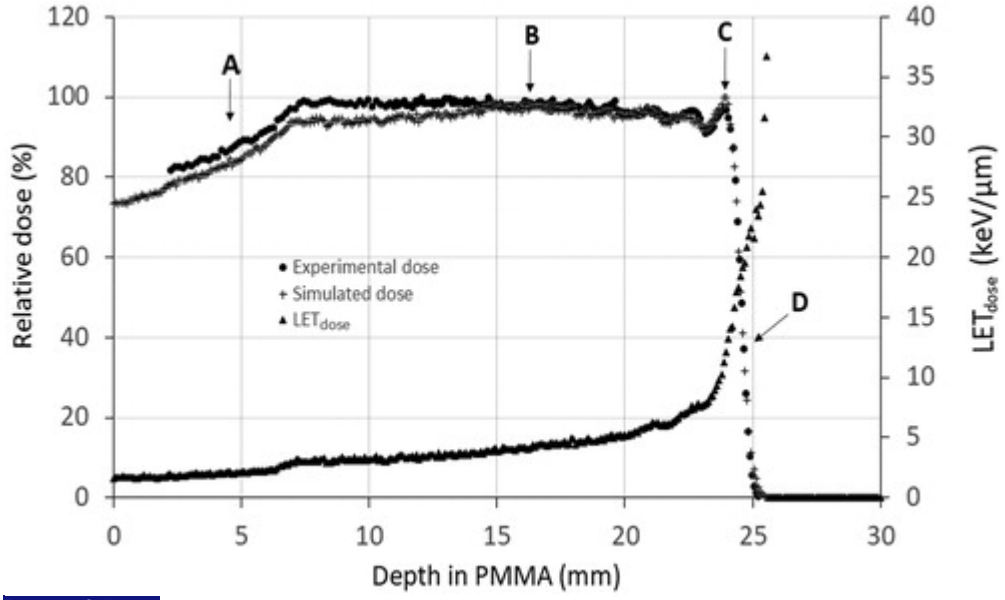

Display full size

Table 1. Irradiation parameters along the 62 MeV therapeutic proton SOBP.

CSVDisplay Table

Figure 1 also comprises the distributions of dose and dose averaged LET (LET_{dose}) as functions of depth in PMMA obtained by the open-source 'Hadrontherapy' application (Cirrone et al. 2005) of the Geant4 Monte Carlo toolkit (Agostinelli et al. 2003; Allison et al. 2006, 2016), and employed to simulate the CATANA facility transport beam line (Cirrone et al. 2004, 2017). The used physical models and data libraries are those that are appropriate for the energy range in radiotherapy. In this figure the ordinate on the left side is related to experimental and simulated dose distributions, while the right one corresponds to dose averaged LET. Detailed description of numerical simulations, conditions and implemented algorithms are given elsewhere (Romano et al. 2014; Petringa et al. 2020). However, the already published results differ slightly from those given in Figure 1 due to minor changes in elements of the transport beam line, such as modulator wheel and range shifter. In numerical simulations, the phantom made of PMMA is split into 10 µm wide slices perpendicular to the axis of the beam.

Irradiations with the 62 MeV/u carbon ions were accomplished at the INFN-LNS 0° beam transport line with the dose averaged LET of ~200 keV/µm, which has the highest effectiveness in cell elimination (Weyrather and Kraft 2004; Ando et al. 2005; Belli et al. 2008). Considering that the carbon ion Bragg peak is very narrow, to avoid complicated and not sufficiently precise positioning of the samples at the pristine peak in order to attain the site providing the wanted LET value, the Bragg peak is somewhat broadened, thus providing sufficiently good reproducibility of the irradiation site (Petrović et al. 2020). This rather widened Bragg peak is achieved by inserting two specially designed ripple filters into the beam transport line (Romano et al. 2014). The wanted irradiation position is found by using PTW Advanced Markus ionizing chamber, as already described, at the PMMA thickness of 5.08 mm, with the relative dose of

99.8 ± 1.6% corresponding to 199.8 ± 3.1 keV/μm. The accuracy of setting the samples before each irradiation is done by GafChromic HS films. Experimentally obtained depth dose distribution of slightly widened beam of carbon ions is presented in Figure 2, including indicated irradiation position.

Figure 2. Measured and simulated depth dose and depth LET_{dose} distribution in Perspex (PMMA) of the 62 MeV/u widened carbon ion beam. Arrow indicates irradiation position. The ordinate on the left side is related to experimental and simulated dose distributions, while the right one corresponds to dose averaged LET.

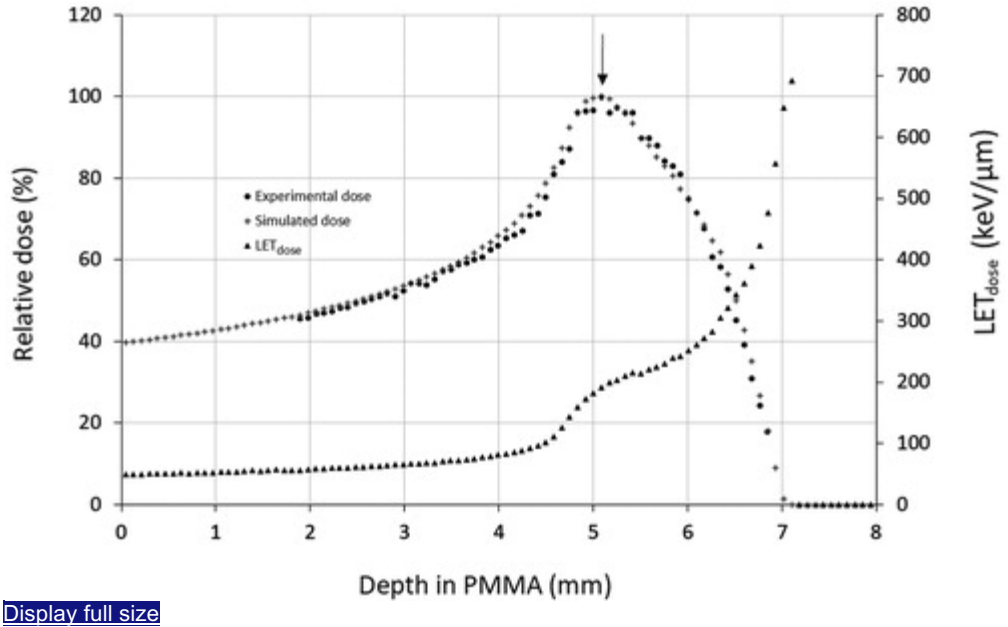

Display full size

In addition, Figure 2 includes the distributions of dose and dose averaged LET (LET_{dose}) as functions of PMMA acquired by simulations of the beam transport of carbon ions using again the Geant4 toolkit, as already described. In this figure the ordinate on the left side corresponds to experimental and simulated dose distributions, while the right one is related to dose averaged LET. Minor discrepancy between previously published data (Romano et al. 2014) and the results presented here are again due to the slight changes in the beam transport line.

The three cell lines are chosen because of similar size and geometry of their nuclei as well as comparable radiosensitivity levels. This is done to minimize differences from geometrical point of view and meet the needs of potential numerical simulations.

Immunofluorescence staining of γ-H2AX foci

After irradiation, cell samples are incubated according to the experimental protocol from 30 minutes to 24 h under standard conditions. Prior to fixation and permeabilization, the cells are washed in phosphate-buffered saline (PBS). They are fixed with 4% paraformaldehyde (PFA) in PBS for 15 minutes at room temperature while for the

permeabilization of cells, 0.2% Triton-X in PBS is used. Further on, the cells are washed with Tris buffer saline (TBS) and blocked with 5% bovine serum albumin (BSA, Fraction V, Sigma-Aldrich Chemie GmbH) for 1 h at room temperature. DNA damage is visualized by staining of γ-H2AX foci with phospho-histone H2AX Serine139 antibody (Alexa Fluor 488, BioLegend Inc. San Diego, California, United States). Specifically, cells are incubated overnight at +4 °C with antibody diluted at 1:500 in 5% BSA-TBST (TBS-Tween 20). Afterwards, samples are rinsed in TBST and dehydrated in 70, 90 and 95% ethanol, and mounted with Vectashield® antifade mounting medium having propidium iodide to stain DNA (Vector Laboratories, USA). Micrographs are acquired using the Leica TCS SP5 II laser confocal microscope (Leica Microsystem CMS GmbH; Wetzlar, Germany). The image processing is done employing the LAS AF Lite software (Leica Microsystem CMS GmbH) while Image J software is employed for the γ-H2AX foci counting.

Statistical analysis

All experiments are performed in duplicate, repeated three times and statistical differences between experimental groups are calculated by Student's *t*-test. Experimental data are presented as means ± SEM (standard error of the mean) while the level of significance is set at $p < .05$.

Results

The principal idea of this study is to follow the loss of γ-H2AX foci in three radioresistant human cancer cell lines, i.e. HTB140, MCF-7 and HTB177 cells, as a function of LET and time. To provide different LET values, cells are irradiated at four irradiation positions along the 62 MeV therapeutic proton SOBP, thus obtaining LET of 2.2, 4.4, 11.3 and 19.3 keV/μm (Figure 1, Table 1). Irradiation positions belong to characteristic parts of the proton SOBP profile: plateau, middle, distal end and distal declining edge, all being of specific interest in clinical practice. The time dependent variation of the number of γ-H2AX foci is analyzed for the LET of 4.4 keV/μm, which is in the middle of the SOBP. Selected post irradiation incubation time points are 0.5, 1, 2, 6 and 24 hours and correspond to the interval needed to track γ-H2AX foci formation process, from initial induction to its disappearance. The obtained results with protons are compared with two types of radiation used in cancer therapy, conventional γ-rays being less efficient and carbon ions of 199.8 keV/μm, considered to be more effective than protons. Moreover, this LET value is reported to be in the range of the most efficient one in cell killing with carbon ions (Weyrather and Kraft 2004; Ando et al. 2005; Fokas et al. 2009; Okayasu 2012). Time points involved in this comparison are 0.5 h, representing the maximal response to irradiations (Ivashkevich et al. 2011; Lu et al. 2019) and 24 h, corresponding to the expression of residual foci (Banáth et al. 2010; Vitti and Parsons 2019). In all irradiations, the dose of 1 Gy is applied.

For protons and carbon ions, respectively, Figures 1 and 2 gather data points representing relative dose as a function of depth in PMMA obtained by experiments and

numerical simulations with the Geant4 toolkit, as well as dose averaged LET as a function of depth in PMMA, also obtained by Geant4 simulations. These data are indispensable for designing the experimental setups and are a part of the overall results attained in this study.

Since cell cycle progression is closely related to DNA damage response to radiation, quantification of cell populations in different phases for each of the three cell lines is performed before irradiation campaigns. Their distributions are given in Figure 3. Between the cell lines there are minor differences within each phase of cell cycle. The majority of cells, which is close to 60%, are in G1 phase, while less than 20% are in S phase.

Figure 3. Cell cycle distributions of HTB140, MCF-7 and HTB177 cells before exposure to radiation.

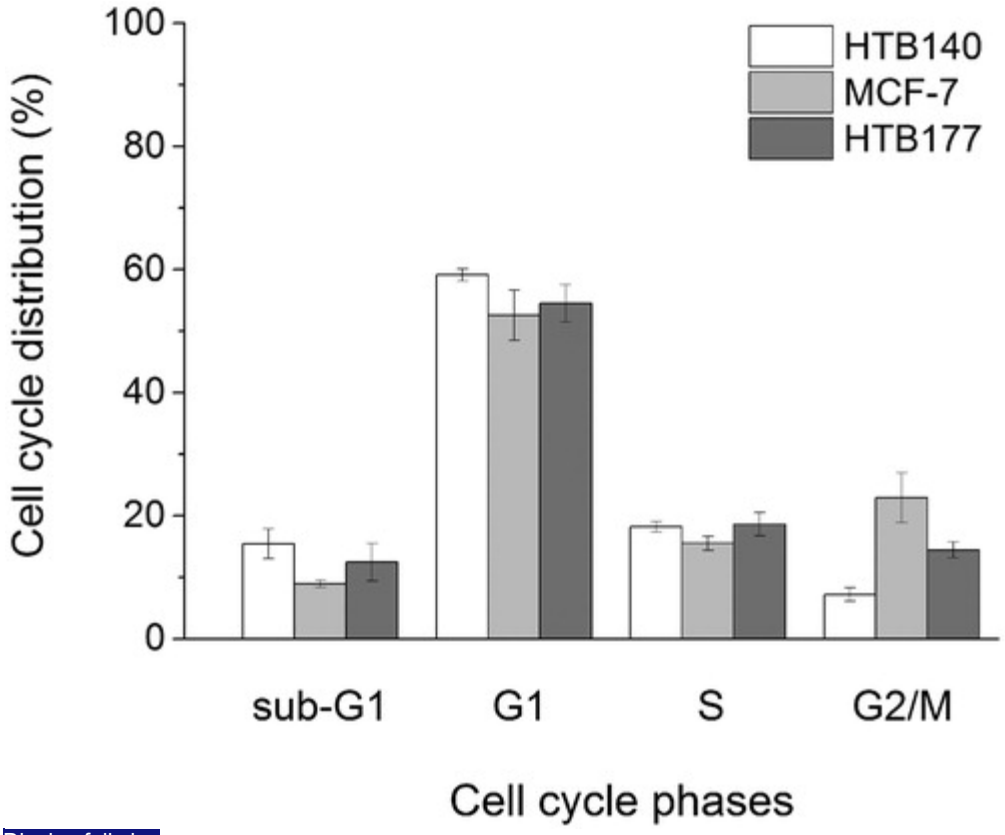

Display full size

The number of γ-H2AX foci per cell at 0.5 h after irradiation with 1 Gy of the 62 MeV proton SOBP, in four irradiation positions defined in Table 1, is presented in Figure 4. At this time point, with the increase of LET the sum of γ-H2AX foci rises for the first three irradiation positions, starting with the LET value of 2.2 keV/μm in the plateau, through 4.4 keV/μm in the middle to 11.3 keV/μm at the distal end, and then it decreases at the irradiation position being at the distal declining edge of SOBP having 19.3 keV/μm. This trend in response to radiation is found for all three tested cell lines with small relative difference between them for each LET (Figure 4). Thus, the estimated average number

of γ-H2AX foci per cell goes from ~20, over ~27 and ~33 to ~29, respectively, while in non-irradiated controls it is ~2.

Figure 4. Number of γ-H2AX foci per cell as a function of LET, 0.5 h after irradiation with 1 Gy of 62 MeV protons along the therapeutic SOBP (irradiation positions A, B, C and D). Results are presented as mean ± SEM (standard error of mean).

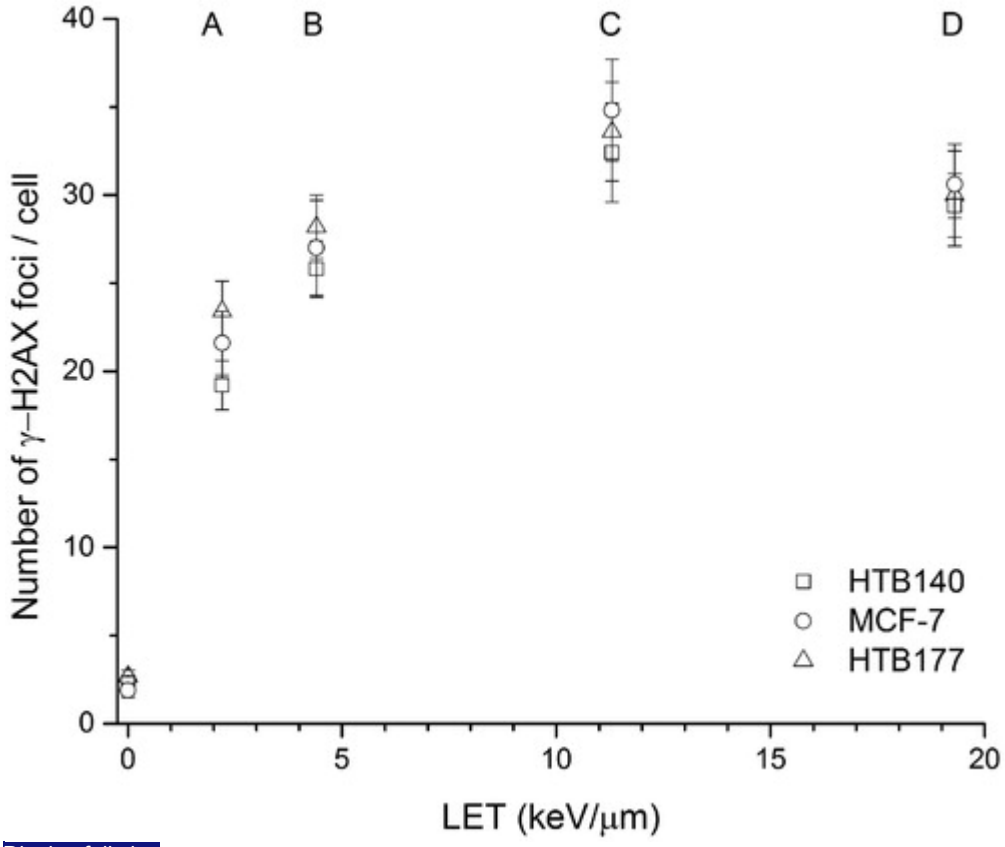

Display full size

To examine the time course of the process of γ-H2AX foci formation and their disappearance, the three cell lines that are exposed to the 62 MeV therapeutic protons in the middle of the SOBP, having LET of 4.4 keV/μm, are further incubated for 0.5, 1, 2, 6 and 24 h. With the assumption that the number of foci per cell is equal to the number of DSB per nucleus (Redon et al. 2009), the irradiation-induced DNA damage is calculated as quantity of DSB per Gy, per Gbp ($Gy^{-1}Gbp^{-1}$). As shown in Figure 5, the time dependent changes in the number of DSB per cell nucleus reveal that the maximum number of DSB can be detected at 0.5 h after irradiation, while later on, it gradually drops. Considering that there is a minor relative discrepancy between the values acquired for the three cell lines, for each time point, their distribution goes on the average from ~4.5, ~3.3, ~3.2, ~2.9 and ~2.5 DNA DSB for 0.5, 1, 2, 6 and 24 h, respectively. At 24 h post irradiation there is an increase in the difference between values for the three cell lines.

Figure 5. Number of DNA DSB ($Gy^{-1}Gbp^{-1}$) at 0.5, 1, 2, 6 and 24 h after irradiation with 1 Gy in the middle of the 62 MeV therapeutic proton SOBP. Results are presented as mean ± SEM (standard error of mean). The assumption is that the number of foci per cell is equal to the number of DSB per nucleus.

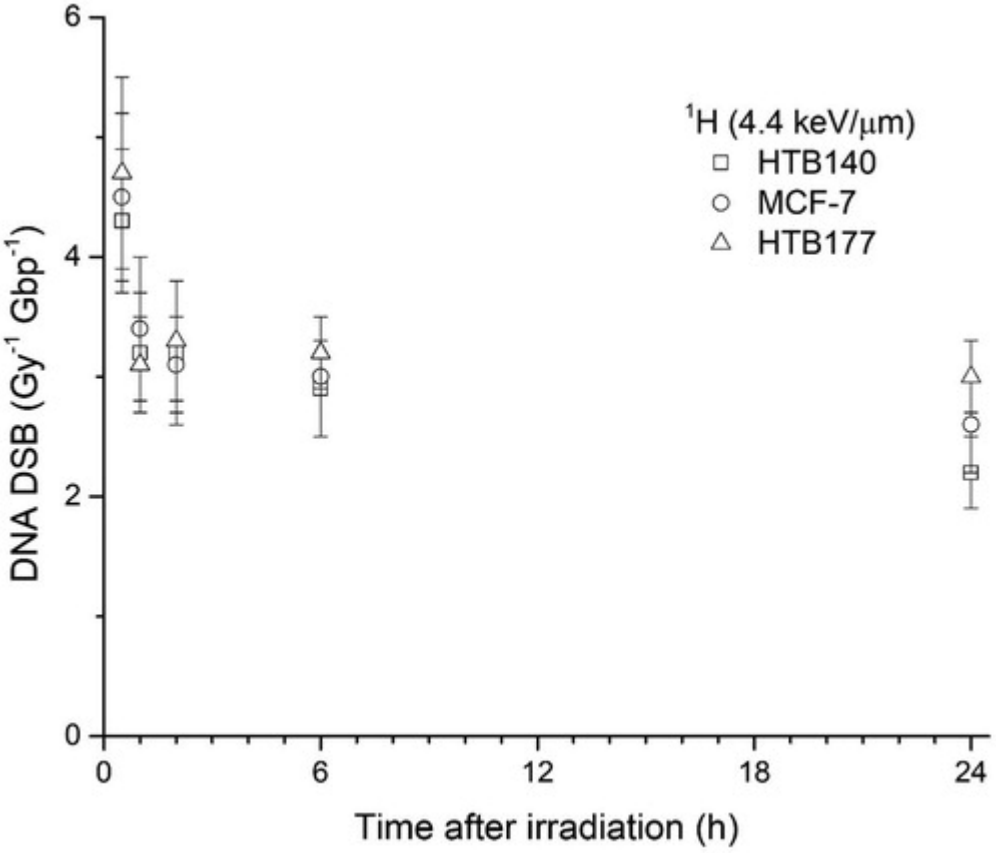

Display full size

Results acquired with protons having LET of 4.4 keV/µm at 0.5 h and 24 h post irradiation are compared to those of γ-rays and carbon ions characterized by LET of ~200 keV/µm, at the same time points, aiming to estimate their relative efficiency. The numbers of DNA DSB at specific time points after irradiation, 0.5 h and 24 h, are given in Table 2. Time point of 0.5 h after irradiation is chosen since it represents the peak of irradiation-induced damage, while the time point of 24 h shows presence of residual foci after DNA repair mechanisms are activated (Rothkamm and Horn 2009; Banáth et al. 2010; Vitti and Parsons 2019). Other time points (1, 2 and 6 h) are not taken into account due to small differences among themselves. The data obtained for γ-rays and carbon ions, for the three cell lines, are mutually and with respect to those of protons quite close, even overlap, so it is not possible to include them all in Figure 5.

Table 2. Number of DNA DSB ($Gy^{-1}Gbp^{-1}$) at 0.5 h and 24 h after irradiation with 1 Gy of γ-rays, protons and carbon ions, calculated under the assumption that the number of foci per cell is equal to the number of DSB per nucleus.

CSVDisplay Table

At 0.5 h after irradiations with γ-rays, all three cell lines have maximum of ~3 DSB ($Gy^{-1}Gbp^{-1}$), while protons and carbon ions induce higher number of foci, giving ~4.5 DSB ($Gy^{-1}Gbp^{-1}$). With respect to non-irradiated control, there is a very significant increase in DNA DSB number in the three cell lines after irradiations with γ-ray, protons and carbon ions ($p < .001$), except for HTB140 cells irradiated with γ-ray where the rise is important ($p < .05$). Comparing to γ-rays, only for MCF-7 cells there is a significant increase in the number of foci induced by proton irradiation ($p < .05$). Carbon ions are considerably more efficient than γ-rays for HTB140 and HTB177 cells ($p < .05$) and not for MCF-7, while with respect to protons the difference for the three cell lines is minor ($p > .05$).

The appearance of the foci that are detected in cells irradiated with carbon ions differs from those induced by other two types of irradiations. They are more voluminous than those induced by protons and particularly γ-rays, as revealed by representative micrographs of single cell nuclei given in Figure 6.

Figure 6. Representative micrographs of single cell nuclei with γ-H2AX foci at 0.5 h after irradiation with 1 Gy of γ-rays, 62 MeV/u mid proton SOBP and carbon ions. Microscope: LeicaTCS SP5 II confocal microscope. Bar: 20 μm.

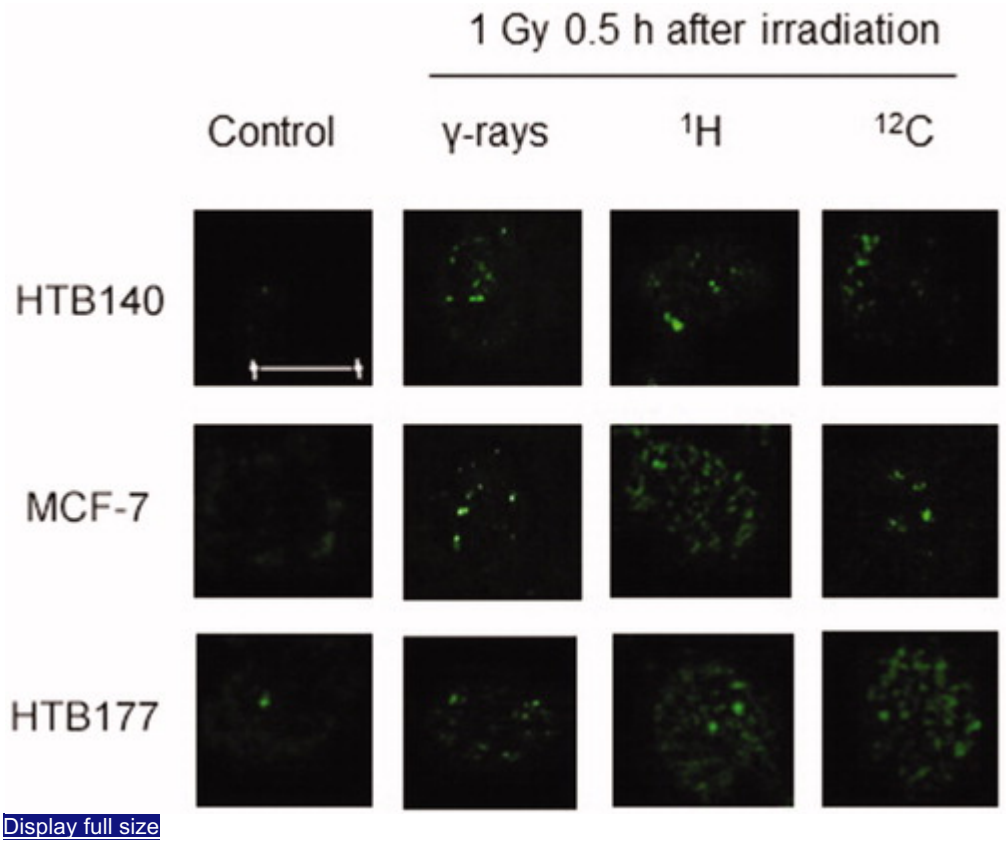

Display full size

With prolonged incubation from 0.5 to 24 h, the number of DNA DSB declines for all cell lines and all applied irradiation types. In regard to nonirradiated control, quite an

important rise of DNA DSB is observed for protons and carbon ions, for all three cell lines ($p < .01$), while for γ-rays there is a significant growth only for MCF-7 cells ($p < .05$). The difference in residual foci is important for protons and carbon ions with respect to γ-rays, with the average number of DSB for γ-rays being ∼1, for protons ∼2.1 and for carbon ions ∼2.6 (Table 2). The lowest number of foci is detected in γ-irradiated cells, with somewhat lower number observed in HTB140 cells than in other two cell lines. In comparison with γ-rays, statistically significant change in the number of DSB after protons is found in HTB140 ($p < .01$), MCF-7 ($p < .05$) and HTB177 ($p < .01$) cells. Carbon ions also induce significantly higher number of DSB compared to γ-rays for HTB140 ($p < .01$), MCF-7 ($p < .05$) and HTB177 ($p < .01$) cells. However, no statistically significant changes are found in the number of DSB between cells irradiated with protons and carbon ions ($p > .05$, Table 2).

Another way to evaluate the relative level of obtained DSB values is to calculate the isodose effect index for γ-H2AX foci formation, which is the ratio at the dose of 1 Gy, of the DNA DSB number ($Gy^{-1}Gbp^{-1}$) induced by protons or carbon ions and conventional γ-rays. The calculated values at 0.5 and 24 h after irradiation are given in Table 3. There is a small difference in the index values regarding protons and carbon ions at 0.5 h postirradiation for all cell lines ($p > .05$), except for the most resistant HTB140 cells, that is largely due to the modest DNA damage capacity of γ-rays (Petrović et al. 2010, 2020). Still this difference is insignificant ($p > .05$). In general, for HTB140 and HTB177 cells, this index reveals higher levels at 24 h after irradiation ($p < .05$, $p < .01$), with an increased difference between protons and carbon ions, being in favor of carbons, although remaining statistically insignificant ($p > 0.05$).

Table 3. Index of isodose effect for γ-H2AX foci formation, that is, DNA DSB number ($Gy^{-1}Gbp^{-1}$) produced by protons or carbon ions with respect to conventional γ-rays, all at the dose level of 1 Gy.

CSVDisplay Table

Discussion

With intention to improve understanding of the effects of LET alterations along the therapeutic proton SOBP, as well as variations with time of these outcomes, consequent differences in DNA DSB induction and resolution are chosen as a specific biological endpoint. To facilitate plausible link of the results obtained *in vitro* with those found *in silico*, it is considered in this study that the measured γ-H2AX foci are directly proportional to DNA DSB (Redon et al. 2009). Cancer cells have an intrinsic radiosensitivity driven by their particular tissue of origin and may acquire mutations which affect radiation response (McMahon et al. 2017). Thus, three different human cancer cell lines, HTB140 melanoma, MCF-7 breast adenocarcinoma and HTB177 non-small lung cancer cells are exposed to irradiations along the 62 MeV therapeutic proton SOBP. In such a way, four irradiation positions and LET values are defined (Table 1). There is quite good agreement between depth dose distributions in PMMA that are

obtained experimentally and by simulations using the Geant4 toolkit. This is particularly visible in the defined irradiation positions and allows to pick up LET values from the depth dose averaged LET curve that is evaluated by simulations (Figure 1). Accurate numerical simulations of the beam transport are essential for successful experimental campaigns and adequate interpretation of results (Romano et al. 2014).

To position the results of proton irradiations within the outcomes of other irradiation species used in cancer therapy, the cell lines are irradiated with conventional γ-rays and carbon ions having LET of ∼200 keV/μm, the first considered to be less while the second more efficient in cell elimination than protons. The LET value for carbon ions is particularly selected since it is reported to be the most powerful in cell killing (Weyrather and Kraft 2004; Ando et al. 2005; Fokas et al. 2009; Okayasu 2012; Petrović et al. 2020). Experimentally obtained depth dose distribution of carbon ions in PMMA matches rather well the one obtained by numerical simulations with Geant4 toolkit (Figure 2). This good accordance permits to choose with reasonable reliability the wanted LET value from the depth dose averaged LET curve, thus defining the corresponding irradiation position.

Considering that different repair pathways triggered by irradiation partly depend on cell cycle stage, it is necessary to evaluate cell populations in various phases of cell cycle for the three cell lines under consideration (Figure 3). The majority of cells are irradiated in G1 phase, thus indicating non-homologous end-joining (NHEJ) as an active repair pathway. Accumulation of cells in G1 phase minimizes contribution from homologous recombination (HR) which is active in S and G2 phase (Mao et al. 2008; Vitti and Parsons 2019).

After being irradiated with protons, all three cell lines respond in a similar manner without showing major fluctuations in γ-H2AX foci number within each LET value, that is, irradiation position along the therapeutic SOBP (Figure 4). When moving irradiation position throughout the proton SOBP, with the rise of LET from the SOBP plateau, through mid-position to the distal end, there is an increase of γ-H2AX foci number per cell (Table 1, Figure 4). However, for the highest LET value, which is on the distal fall off part of SOBP, the foci number per cell drops. γ-H2AX foci assay seems to be a surrogate for DNA damage, because it detects not only irradiation induced DSB but also those produced by replication. These types of damage are repaired by different cellular pathways. Certain studies dedicated to processing of clustered DNA damage, have shown that more than 50% of DSB induced by low LET radiation are rejoined within 30 minutes and that additional DSB are formed post-irradiation (Gulston et al. 2004). Moreover, it is unclear whether the loss of visible γ-H2AX foci precisely correlates with the final step in the rejoining of DNA strand breaks or it happens with delay. Although γ-H2AX foci analysis is restricted, this does not exclude its usefulness for monitoring the process of DSB repair as long as the imperfections are considered carefully during interpretation of results (Löbrich et al. 2010). Good experience of the use of this analysis is shown for irradiations with protons (Zlobinskaya et al. 2012). Taking into account benefits and limitations of γ-H2AX foci assay, in this study, we consider that the foci are fully formed by ∼0.5 h after irradiations (Ivashkevich et al. 2011; Lu et al. 2019).

Variations in the amount and complexity of DNA lesions produced along the proton Bragg peak are still rather controversial and additional investigations on how particular DNA repair pathways contribute to the formation of clustered DNA damage are needed. It is suggested that more pronounced lethal effects of protons at the distal edge and particularly distal fall off part of SOBP (irradiation positions C and D in Figures 1 and 4) is most probably related to their capability to induce rather complex or clustered DSB. This type of irradiation-induced damage is more difficult to repair and is considered to be consequence of higher LET and truck structure of protons (Calugaru et al. 2011; Oeck et al. 2018).

Our previous observation is that melanoma, breast adenocarcinoma and non-small lung cancer cell lines differ in radiosensitivity showing dissimilar survival levels after irradiation with protons (Petrović et al. 2020; Ristić Fira et al. 2020). It is reported that HTB140 melanoma cells are the most radioresistant to protons when compared to either MCF-7 breast carcinoma or HTB177 non-small lung cancer cells. These findings are supported by other literature data suggesting that HTB140 cells belong to the group of highly radioresistant cancer cell lines (Fertil and Malaise 1981; Petrović et al. 2006, 2010). Although there are differences in radiosensitivity for the three cell lines, small variations in foci formation, which are all within the standard error of the mean, are detected for the same LET values. This leads to the presumption that at 0.5 h after irradiation cells having different radiosensitivity levels would produce a rather close number of foci, therefore not expressing their inherent nature, that is, radiosensitivity degree. Such behavior is in favor of performing validation of the results acquired through numerical simulations using Geant4-DNA by those experimentally obtained, since this toolkit does not consider inherent differences between cell lines (Sakata et al. 2020).

Monitoring the phosphorylation of histone H2AX is employed to visualize and quantify the kinetics of DNA DSB evolution due to time-dependent repair events (Oeck et al. 2018). Rather than examining only the initial rise of DNA DSB, post-irradiation time of 24 h is often used to distinguish lesions that have been repaired from those that are persistent, more difficult for the cell to restore and are therefore considered as probably lethal. Consequently, quantification of γ-H2AX foci is followed over the defined time interval starting from 0.5 h up to 24 h after irradiation. Since the loss of clonogenic capacity after irradiation could be explained by the inability of the affected cell to repair the damage, the number of residual DNA DSB is seen as a marker of irreparable DNA damage and therefore is the indicator of cellular fate after irradiation (Rothkamm and Horn 2009; Banáth et al. 2010). The obtained number of proton induced DSB is in agreement with other reports in regard to both normal and cancer cells (Zlobinskaya et al. 2012; Sakata et al. 2019). The kinetics of γ-H2AX foci, i.e. time variation of DNA DSB number, exhibits a drop after the maximum at 0.5 h, throughout 1, 2, 6 and 24 h (Figure 5).

The presence of DSB at longer time points is due to DSB which are more difficult to repair, but also to late forming DSB issued through processing of complex or clustered DNA damage (Vitti and Parsons 2019). For each time point, there is a small difference between the numbers of DSB obtained for the three cell lines and are within the

standard error of the mean. Still there is a rise in the difference between values for the three cell lines at 24-h postirradiation. In addition, HTB140 cells show lower number of residual DSB compared to other two cell lines, pointing out their higher efficacy in repairing damage that arises after proton irradiation. This is reflected in greater survival level of HTB140 cells that explains their higher radioresistance in general (Petrović et al. 2020). With the prolonged incubation period up to 24 h, the inherent nature of cell lines becomes apparent through increased differences in the number of persisting DNA DSB. Described trend will later on increase and result in clonogenic survival that is different among the three cell lines (Banáth et al. 2010; Petrović et al. 2020).

Since repair events and cellular destiny after irradiations with higher-LET particles are still quite unclear, we have included carbon ions to compare their effects with those of protons as well as with conventional γ-ray irradiation and thus better understand the radiosensitivity of the tested cell lines (Table 2). At a shorter time interval, which is 0.5 h in this study, carbon ions produce more damage to the tested cell lines than γ-rays, while with regard to protons the difference is small. Irradiations with protons provoked more foci than γ-rays in all cell lines at 0.5 h after irradiations. Counting foci at 24 h after irradiation points out that variation in residual foci is significant for protons and carbon ions with respect to γ-rays, while mutually the difference is minor. Index of the isodose effect for γ-H2AX foci formation is introduced in a similar way as isodose relative biological effectiveness in cell survival studies (Shim et al. 2016). Thus, one can estimate the relative efficiency of DNA DSB production of a chosen radiation specie with respect to conventional one. There is a minor variation in index of isodose effect within protons or carbon ions, as well as when comparing protons to carbon ions, for the three cell lines, at 0.5 h (Table 3). At 24 h after irradiations, the index increases with respect to the time point of 0.5 h, since it is influenced by persistent residual foci that lead to the final outcome – surviving fraction. Larger differences in the index at 24 h are seen within protons or carbon ions, as well as for protons vs. carbon ions, for the three cell lines. This conduct, which is not noticed at 0.5 h, implies that as time goes by up to 24 h inherent individual characteristics of each cell line become visible, having at the origin their specific repair capacities. Major discrepancy is produced for all comparisons with respect to HTB 140 cells, mainly due to low number of DNA DSB produced by γ-rays.

Compared to protons, carbon ions do not produce significantly higher number of γ-H2AX foci, as it might be expected because of their more powerful physical properties that result in higher cell killing capacity. The experiments performed in this study required lower radiation dose of 1 Gy for the quantification of γ-H2AX foci per single-cell nucleus, since higher doses could trigger accumulation and overlapping of fluorescent signal. Still, no major differences in residual foci count are observed after carbon ions compared to protons as it could be assumed according to relevant survival data. Our previous findings indicate higher cell killing ability of carbon ions compared to protons in HTB140, MCF-7 and HTB177 cells that is explained by different track structure and more complex damage produced by carbon ions (Schipler and Iliakis 2013; Lopez Perez et al. 2019; Petrović et al. 2020). In contrast to γ-rays, which induce DSB with mostly random distribution of small foci within the nucleus, data obtained for heavy ion particles demonstrate the existence of clustered DSB (foci) along the particle track (Weber and Kraft 2009; Lopez Perez et al. 2016; Friedland et al. 2017). As shown by

Monte Carlo simulations, these complex DNA lesions may comprise DSB, but also SSB and base damages (Hagiwara et al. 2019).

In the present work we observe that γ-H2AX foci arising after carbon ion irradiations are larger and with different, more irregular shape compared to those induced by either γ-rays or protons, which produce foci that are smaller and more rounded (Figure 6). Even though a lower irradiation dose is applied, carbon ions induce DNA lesions that are in closer proximity to one another, causing the overlapping of fluorescent signals. Therefore, the induction of higher amount of DSB may result in underestimation of their number due to limitations of the detection method which is unable to distinguish foci that are too close to each other. Moreover, clustered DNA lesions could also be the reason for the higher number of residual foci after carbon ions compared to protons and especially γ-rays (Table 2). Delay in resolution of DNA lesions, as reflected by residual foci, could be due to complexity of DNA damage that is difficult to repair (Suzuki et al. 2000; Oeck et al. 2018; Lopez Perez et al. 2019). For high LET heavy ion irradiations, it has been reported that with the rise of LET complex DNA damage increases in irradiated cells. These are mostly unrepairable lesions that provoke either chromosome aberrations or lead cells into senescence (Asaithamby et al. 2011; Zhang et al. 2016). It is necessary to make distinction between unrepairable, highly complex DNA damage produced by heavy ions and complex DNA damage sights created by protons which are probably less complex in itself and in fact repairable (Sage and Shikazono 2017; Vitti and Parsons 2019).

A variety of activated biological mechanisms determines cellular response to radiation with DNA repair processes being the most important (Barbieri et al. 2019). The final fate of irradiated cell is defined by complex cascades of pathways resulting either in overcoming damage and consequently cell survival or inefficiency of repair mechanisms leading to mutations and cell death (Belka 2006). DNA damage induced by radiation might arise either as a consequence of direct interaction between irradiation and DNA molecule or be mediated by free radicals generated through radiolysis of water (Goodhead 1994; Wallace 1998; Mavragani et al. 2016). It has been shown that in contrast to low-LET irradiations which produce predominantly indirect damage to DNA, high-LET irradiations are capable to directly insult DNA molecule (Roots and Okada 1972; Mavragani et al. 2016). The complexity of interplay of different pathways involved in DNA damage response including different types of cell death, i.e. apoptosis, mitotic catastrophe or senescence makes it difficult to predict final outcome of damage caused by irradiation. Considering that cellular destiny after irradiation is likely to be dependent on cell line, it is difficult to make a unique mechanistic model of cellular response to radiation (Barbieri et al. 2019). Even though numerical modeling of radiation-induced DNA damage has proven to be successful, in order to improve current models based mostly on physical interactions, further attempts are orientated toward better understanding of the DNA damage response mechanisms. Biological data on irradiation response of different cancer cells are therefore important as they could be compared with simulated results, especially when it comes to the effects of various radiation qualities which result in DNA lesions of diverse complexities (Sakata et al. 2019). Data presented in this study, particularly those belonging to ‘early effects’ at 0.5 h, with no significant difference between the three cell lines, would be valuable for

comparisons with simulation data and contribute to the development of more accurate *in silico* tools.

Conclusion

In the present study HTB140, MCF-7 and HTB177 cell lines are selected because of similar geometries and comparable dimensions of their nuclei as well as comparable radiosensitivity. By visualizing DNA DSB produced in cells after irradiations along the therapeutic proton SOBP, thus obtaining different LET values, we demonstrate that with the rise of LET up to the distal end of SOBP, the number of γ-H2AX foci rises, while passing to the distal declining edge it drops. For each LET used, the number of foci for the three cell lines is very close. Choosing as the irradiation position the one in the middle of the proton SOBP, time dependence of formation and disappearance of DNA DSB is followed revealing that their number gradually decreases with time. While the 'early effects' after irradiation display no significant difference between the three cell lines, those related to the formation of residual foci start to express the inherent nature of tested cells, therefore increasing discrepancy between them. When compared to γ-rays, protons express higher effectiveness when inducing DSB in all three cell lines. Irradiations with carbon ions show their larger capacity, with respect to other two irradiation species, to induce DNA damage as illustrated by very prominent fluorescent signal. Of note, in terms of DSB number, although not expected, tested cell lines responded similarly to carbon ions and protons. Since carbon ions are more effective in elimination of analyzed cancer cells as previously demonstrated by survival data, this could be explained by their ability to cause more complex DSB which are hard to distinguish due to proximity of ionizing events and consequent foci overlapping. With aim to implement patient-specific DNA damage response into available numerical models, these results would be used for validation of the Geant4-DNA simulation toolkit and thus help to develop personalized cancer therapies.

Disclosure statement

No potential conflict of interest was reported by the author(s).

Additional information

Funding

This work was financially supported by the Ministry of Education, Science and Technological Development of Serbia and by Fondo Affari Internazionali (FAI) of the INFN-LNS. The research leading to these results has also received funding from the European Union HORIZIN2020 research and innovation program under [Grant Agreement no 654002 ENSAR2]. The authors wish also to acknowledge financial

support from CNRS PICS #8070 France – Serbia Project and MAECI PGR No. 00794 Italy – Serbia Project.

Notes on contributors

Otilija Keta

Otilija Keta received her Ph.D. from the University of Belgrade, Faculty of Biology. Presently she is engaged as Research Assistant Professor at the Vinča Institute of Nuclear Sciences of the University of Belgrade.

Vladana Petković

Vladana Petković received her Master degree from the University of Belgrade, Faculty of Biology. She is a PhD student at the University of Belgrade, Faculty of Biology, working on her thesis at the Vinča Institute of Nuclear Sciences of the University of Belgrade.

Pablo Cirrone

Pablo Cirrone received his PhD in Physics at the University of Catania (I). He is a Senior Researcher at the INFN Italian Institute for Nuclear Physics and Professor of the 'Medical Physics' class at the Catania University. He is an expert of Hadrontherapy, laser-driven acceleration and diagnostic, dosimetry of ionization radiation and Monte Carlo simulations.

Giada Petringa

Giada Petringa received her PhD in Physics from the University of Catania (I). She is an expert in diagnostics and dosimetry for clinical and laser-driven proton/ions beams. She has a large experience in Monte Carlo simulations and she is a member of the Geant4 international collaboration.

Giacomo Cuttone

Giacomo Cuttone is Research Director at the INFN Italian Institute for Nuclear Physics and Professor of the 'Accelerator Physic' class at the Catania University. He is also the former Director of INFN-LNS. He is expert of accelerator physics, hadrontherapy and dosimetry for ionizing radiation.

Dousatsu Sakata

Dousatsu Sakata received his PhD from University of Tsukuba, Tsukuba, Japan. He is a Research Associate in the National Institute of Radiological Sciences, Japan. He is involved in development of the Geant4 simulation toolkit, in particular, radiobiological modeling.

Wook-Geun Shin

Wook-Geun Shin received his PhD in radiobiological simulation using MC method from Bordeaux University. His research interests are radiobiology, radiation therapy, and comprehensive MC simulation. He is also a member of Geant4 and Geant4-DNA collaboration group.

Sebastien Incerti

Sebastien Incerti received his PhD from Blaise Pascal University, Clermont-Ferrand, France. He is a Research Director in the National Institute of Nuclear and Particle Physics (IN2P3) of the National Center for Scientific Research (CNRS), France. He is

involved in development of the Geant4 general purpose and open-source particle-matter simulation toolkit.

Ivan Petrović

Ivan Petrović received his PhD in Nuclear Physics from the Univesity of Paris XI – South (Orsay), France. He is a Research Professor in the Department of Physics at the Vinča Institute of Nuclear Sciences of the University of Belgrade, Serbia, and is actively involved in research and teaching.

Aleksandra Ristić Fira

Aleksandra Ristić Fira received her PhD in Molecular Biology from the University of Belgrade, Faculty of Biology. She is a Research Professor at the University of Belgrade, Vinča Institute of Nuclear Sciences. She is head of Laboratory of radiation biology and is actualy engaged in teaching and research.

Previous article**View** latest articles**Next** article

References

1. Agostinelli S, Allison J, Amako K, Apostolakis J, Araujo H, Arce P, Asai M, Axen D, B anerjee S, Barrand G, et al. 2003. Geant4—a simulation toolkit. Nucl Instrum Meth A. 506:250–303. [Google Scholar]
2. Allison J, Amako K, Apostolakis J, Araujo H, Dubois PA, Asai M, Barrand G, Capra R , Chauvie S, Chytracek R, et al. 2006. Geant4 developments and applications. IEEE Trans Nucl Sci. 53(1):270–278. [Crossref], [Web of Science ®], [Google Scholar]
3. Allison J, Amako K, Apostolakis J, Arce P, Asai M, Aso T, Bagli E, Bagulya A, Banerj ee S, Barrand G, et al. 2016. Recent Developments in Geant4. Nucl Instrum Meth A. 835:186–225. [Crossref], [Web of Science ®], [Google Scholar]
4. Ando K, Koike S, Uzawa A, Takai N, Fukawa T, Furusawa Y, Aoki M, Miyato Y. 2005. Biological gain of carbon-ion radiotherapy for the early response of tumor growth delay and against early response of skin reaction in mice. J Radiat Res. 46(1):51–57. [Crossref], [PubMed], [Web of Science ®], [Google Scholar]
5. Asaithamby A, Hu B, Chen DJ. 2011. Unrepaired clustered DNA lesions induce chromosome breakage in human cells. Proc Natl Acad Sci USA. 108(20):8293–8298. [Crossref], [PubMed], [Web of Science ®], [Google Scholar]
6. Banáth JP, Klokov D, Macphail SH, Banuelos CA, Olive PL. 2010. Residual gammaH2AX foci as an indication of lethal DNA lesions. BMC Cancer. 10:4. [Crossref], [PubMed], [Web of Science ®], [Google Scholar]
7. Barbieri S, Babini G, Morini J, Friedland W, Buonanno M, Grilj V, Brenner DJ, Ottolen ghi A, Baiocco G. 2019. Predicting DNA damage foci and their experimental readout with 2D microscopy: a unified approach applied to photon and neutron exposures. Sci Rep. 9(1):14019. [Crossref], [PubMed], [Google Scholar]
8. Belka C. 2006. The fate of irradiated tumor cells. Oncogene. 25(7):969–971. [Crossref], [PubMed], [Web of Science ®], [Google Scholar]
9. Belli M, Bettega D, Calzolari P, Cherubini R, Cuttone G, Durante M, Esposito G, Furu sawa Y, Gerardi S, Gialanella G, et al. 2008. Effectiveness of monoenergetic and spread-out Bragg peak carbon-ions for inactivation of various normal and tumour human cell lines. J Radiat Res. 49(6):597–607. [Crossref], [PubMed], [Web of Science ®], [Google Scholar]

10. Bernal MA, Bordage MC, Brown JMC, Davídková M, Delage E, El Bitar Z, Enger SA, Francis Z, Guatelli S, Ivanchenko VN, et al. 2015. Track structure modeling in liquid water: A review of the Geant4-DNA very low energy extension of the Geant4 Monte Carlo simulation toolkit. Phys Med. 31(8):861–874. [Crossref], [PubMed], [Web of Science ®], [Google Scholar]
11. Calugaru V, Nauraye C, Noël G, Giocanti N, Favaudon V, Mégnin-Chanet F. 2011. Radiobiological characterization of two therapeutic proton beams with different initial energy spectra used at the Institut Curie Proton Therapy Center in Orsay. Int J Radiat Oncol Biol Phys. 81(4):1136–1143. [Crossref], [PubMed], [Web of Science ®], [Google Scholar]
12. Chatzipapas KP, Papadimitroulas P, Emfietzoglou D, Kalospyros SA, Hada M, Georg akilas AG, Kagadis GC. 2020. Ionizing radiation and complex DNA damage: quantifying the radiobiological damage using Monte Carlo simulations. Cancers. 12(4):799. [Crossref], [Web of Science ®], [Google Scholar]
13. Choi J, Kang JO. 2012. Basics of particle therapy II: relative biological effectiveness. Radiat Oncol J. 30(1):1–13. [Crossref], [PubMed], [Google Scholar]
14. Cirrone GAP, Cuttone G, Guatelli S, Lo Nigro S, Mascialino B, Pia MG, Raffaele L, Russo G, Sabini MG. 2005. Implementati on of a new Monte Carlo-Geant4 simulation tool for the development of a proton therapy beamline and verification of the related dose distributions. IEEE Trans Nucl Sci. 52(1):262–265. [Crossref], [Web of Science ®], [Google Scholar]
15. Cirrone G, Cuttone G, Lojacono PA, Lo Nigro S, Mongelli V, Patti IV, Privitera G, Raffaele L, Rifuggiato D, Sabini MG, et al. 2004. A 62-MeV proton beam for the treatment of ocular melanoma at Laboratori Nazionali del Sud-INFN. IEEE Trans Nucl Sci. 51(3):860–865. [Crossref], [Web of Science ®], [Google Scholar]
16. Cirrone GAP, Cuttone G, Raffaele L, Salamone V, Avitabile T, Privitera G, Spatola C, Amico AG, Larosa G, Leanza R, et al. 2017. Corrigendum: clinical and research activities at the CATANA facility of INFN-LNS: from the conventional hadrontherapy to the laser-driven approach. Front Oncol. 7:247. [Crossref], [PubMed], [Web of Science ®], [Google Scholar]
17. Cooke SL, Temple J, Macarthur S, Zahra MA, Tan LT, Crawford RAF, Ng CKY, Jime nez-Linan M, Sala E, Brenton JD. 2011. Intra-tumour genetic heterogeneity and poor chemoradiotherapy response in cervical cancer. Br J Cancer. 104(2):361–368. [Crossref], [PubMed], [Web of Science ®], [Google Scholar]
18. Durante M, Orecchia R, Loeffler JS. 2017. Charged-particle therapy in cancer: clinical uses and future perspectives. Nat Rev Clin Oncol. 14(8):483–495. [Crossref], [PubMed], [Web of Science ®], [Google Scholar]
19. Fertil B, Malaise EP. 1981. Inherent cellular radiosensitivity as a basic concept for human tumor radiotherapy. Int J Radiat Oncol Biol Phys. 7(5):621–629. [Crossref], [PubMed], [Web of Science ®], [Google Scholar]
20. Fokas E, Kraft G, An H, Engenhart-Cabillic R. 2009. Ion beam radiobiology and cancer: time to update ourselves. Biochim Biophys Acta. 1796(2):216–229. [Crossref], [PubMed], [Web of Science ®], [Google Scholar]
21. Friedland W, Schmitt E, Kundrát P, Dingfelder M, Baiocco G, Barbieri S, Ottolenghi A . 2017. Comprehensive track-structure based evaluation of DNA damage by light

ions from radiotherapy-relevant energies down to stopping. Sci Rep. 7:45161. [Crossref], [PubMed], [Web of Science ®], [Google Scholar]
22. Goodhead DT. 1994. Initial events in the cellular effects of ionizing radiations: clustered damage in DNA. Int J Radiat Biol. 65(1):7–17. [Taylor & Francis Online], [Web of Science ®], [Google Scholar]
23. Goodhead DT, Thacker J, Cox R. 1993. Weiss Lecture. Effects of radiations of different qualities on cells: molecular mechanisms of damage and repair. Int J Radiat Biol. 63(5):543–556. [Taylor & Francis Online], [Web of Science ®], [Google Scholar]
24. Gulston M, de Lara C, Jenner T, Davis E, O'Neill P. 2004. Processing of clustered DNA damage generates additional double-strand breaks in mammalian cells post-irradiation. Nucleic Acids Res. 32(4):1602–1609. [Crossref], [PubMed], [Web of Science ®], [Google Scholar]
25. Hagiwara Y, Oike T, Niimi A, Yamauchi M, Sato H, Limsirichaikul S, Held KD, Nakano T, Shibata A. 2019. Clustered DNA double-strand break formation and the repair pathway following heavy-ion irradiation. J Radiat Res. 60(1):69–79. [Crossref], [PubMed], [Web of Science ®], [Google Scholar]
26. Ilicic K, Combs SE, Schmid TE. 2018. New insights in the relative radiobiological effectiveness of proton irradiation. Radiat Oncol. 13(1):6. [Crossref], [PubMed], [Google Scholar]
27. Incerti S, Baldacchino G, Bernal M, Capra R, Champion C, Francis Z, Guèye P, Mantero A, Mascialino B, Moretto P, et al. 2010. The Geant4-DNA project. Int J Model Simul Sci Comput. 01(02):157–178. [Crossref], [Google Scholar]
28. Incerti S, Champion C, Tran HN, Karamitros M, Bernal M, Francis Z, Ivanchenko V, Mantero A. 2013. Energy deposition in small-scale targets of liquid water using the very low energy electromagnetic physics processes of the Geant4 toolkit. Nucl Instruments Methods Phys Res Sect B Beam Interact Mater Atoms. 306:158–164. [Crossref], [Web of Science ®], [Google Scholar]
29. Incerti S, Douglass M, Penfold S, Guatelli S, Bezak E. 2016. Review of Geant4-DNA applications for micro and nanoscale simulations. Phys Med. 32(10):1187–1200. [Crossref], [PubMed], [Web of Science ®], [Google Scholar]
30. Incerti S, Ivanchenko A, Karamitros M, Mantero A, Moretto P, Tran HN, Mascialino B, Champion C, Ivanchenko VN, Bernal MA, et al. 2010. Comparison of Geant4 very low energy cross section models with experimental data in water. Med Phys. 37(9):4692–4708. [Crossref], [PubMed], [Web of Science ®], [Google Scholar]
31. Incerti S, Kyriakou I, Bernal MA, Bordage MC, Francis Z, Guatelli S, Ivanchenko V, Karamitros M, Lampe N, Lee SB, et al. 2018. Geant4-DNA example applications for track structure simulations in liquid water: a report from the Geant4-DNA Project. Med Phys. 45:e722–e739. [Crossref], [Web of Science ®], [Google Scholar]
32. International Atomic Energy Agency (IAEA) 2000. Absorbed dose determination in external beam radiotherapy: an international code of practice for dosimetry based on standards of absorbed dose to water. Technical Reports Series No. 398, IAEA, Vienna. [Google Scholar]
33. Ivashkevich AN, Martin OA, Smith AJ, Redon CE, Bonner WM, Martin RF, Lobachevsky PN. 2011. γH2AX foci as a measure of DNA damage: a computational approach to automatic analysis. Mutat Res. 711(1–2):49–60. [Crossref], [PubMed], [Web of Science ®], [Google Scholar]

34. Liu H, Chang JY. 2011. Proton therapy in clinical practice. Chin J Cancer. 30(5):315–326. [Crossref], [PubMed], [Google Scholar]
35. Löbrich M, Shibata A, Beucher A, Fisher A, Ensminger M, Goodarzi AA, Barton O, Jeggo PA. 2010. gammaH2AX foci analysis for monitoring DNA double-strand break repair: strengths, limitations and optimization. Cell Cycle. 9(4):662–669. [Taylor & Francis Online], [Web of Science ®], [Google Scholar]
36. Loeffler JS, Durante M. 2013. Charged particle therapy-optimization, challenges and future directions. Nat Rev Clin Oncol. 10(7):411–424. [Crossref], [PubMed], [Web of Science ®], [Google Scholar]
37. Lopez Perez R, Best G, Nicolay NH, Greubel C, Rossberger S, Reindl J, Dollinger G, Weber KJ, Cremer C, Huber PE. 2016. Superresolution light microscopy shows nanostructure of carbon ion radiation-induced DNA double-strand break repair foci. Faseb J. 30(8):2767–2776. [Crossref], [PubMed], [Web of Science ®], [Google Scholar]
38. Lopez Perez R, Nicolay NH, Wolf JC, Frister M, Schmezer P, Weber KJ, Huber PE. 2019. DNA damage response of clinical carbon ion versus photon radiation in human glioblastoma cells. Radiother Oncol. 133:77–86. [Crossref], [PubMed], [Web of Science ®], [Google Scholar]
39. Lu H, Saha J, Beckmann PJ, Hendrickson EA, Davis AJ. 2019. DNA-PKcs promotes chromatin decondensation to facilitate initiation of the DNA damage response. Nucleic Acids Res. 47(18):9467–9479. [Crossref], [PubMed], [Web of Science ®], [Google Scholar]
40. Malouff TD, Mahajan A, Krishnan S, Beltran C, Seneviratne DS, Trifiletti DM. 2020. Carbon ion therapy: a modern review of an emerging technology. Front Oncol. 10:82. [Crossref], [PubMed], [Web of Science ®], [Google Scholar]
41. Mao Z, Bozzella M, Seluanov A, Gorbunova V. 2008. DNA repair by nonhomologous end joining and homologous recombination during cell cycle in human cells. Cell Cycle. 7(18):2902–2906. [Taylor & Francis Online], [Web of Science ®], [Google Scholar]
42. Mavragani IV, Laskaratou DA, Frey B, Candéias SM, Gaipl US, Lumniczky K, Georgakilas AG. 2016. Key mechanisms involved in ionizing radiation-induced systemic effects. A current review. Toxicol Res. 5(1):12–33. [Crossref], [Web of Science ®], [Google Scholar]
43. McMahon SJ, McNamara AL, Schuemann J, Paganetti H, Prise KM. 2017. A general mechanistic model enables predictions of the biological effectiveness of different qualities of radiation. Sci Rep. 7(1):10790. [Crossref], [PubMed], [Google Scholar]
44. Mein S, Dokic I, Klein C, Tessonnier T, Böhlen TT, Magro G, Bauer J, Ferrari A, Parodi K, Haberer T, et al. 2019. Biophysical modeling and experimental validation of relative biological effectiveness (RBE) for 4He ion beam therapy. Radiat Oncol. 14(1):123. [Crossref], [PubMed], [Google Scholar]
45. Nickoloff JA, Sharma N, Taylor L. 2020. Clustered DNA double-strand breaks: biological effects and relevance to cancer radiotherapy. Genes. 11(1):99. [Crossref], [Web of Science ®], [Google Scholar]

46. Nikjoo H, O'Neill P, Terrissol M, Goodhead DT. 1994. Modelling of radiation-induced DNA damage: the early physical and chemical event. Int J Radiat Biol. 66(5):453–457. [Taylor & Francis Online], [Web of Science ®], [Google Scholar]
47. Oeck S, Szymonowicz K, Wiel G, Krysztofiak A, Lambert J, Koska B, Iliakis G, Timm ermann B, Jendrossek V. 2018. Relating linear energy transfer to the formation and resolution of DNA repair foci after irradiation with equal doses of X-ray photons, plateau, or Bragg-peak protons. IJMS. 19(12):3779. [Crossref], [Google Scholar]
48. Okayasu R. 2012. Repair of DNA damage induced by accelerated heavy ions-a mini review. Int J Cancer. 130(5):991–1000. [Crossref], [PubMed], [Web of Science ®], [Google Scholar]
49. Ostashevsky JY. 1989. A model relating cell survival to DNA fragment loss and unrepaired double-strand breaks. Radiat Res. 118(3):437–466. [Crossref], [PubMed], [Web of Science ®], [Google Scholar]
50. Paganetti H. 2014. Relative biological effectiveness (RBE) values for proton beam therapy. Variations as a function of biological endpoint, dose, and linear energy transfer. Phys Med Biol. 59(22):R419–72. [Crossref], [PubMed], [Web of Science ®], [Google Scholar]
51. Paganetti H. 2018. Proton relative biological effectiveness - uncertainties and opportunities. Int J Part Ther. 5(1):2–14. [Crossref], [PubMed], [Google Scholar]
52. Paganetti H, Niemierko A, Ancukiewicz M, Gerweck LE, Goitein M, Loeffler JS, Suit HD. 2002. Relative biological effectiveness (RBE) values for proton beam therapy. Int J Radiat Oncol Biol Phys. 53(2):407–421. [Crossref], [PubMed], [Web of Science ®], [Google Scholar]
53. Petringa G, Pandola L, Agosteo S, Catalano R, Colautti P, Conte V, Cuttone G, Fan K, Mei Z, Rosenfeld A, et al. 2020. Monte Carlo implementation of new algorithms for the evaluation of averaged-dose and -track linear energy transfers in 62 MeV clinical proton beams. Phys Med Biol. 65(23):235043. [Crossref], [PubMed], [Web of Science ®], [Google Scholar]
54. Petrović I, Ristić
Fira A, Keta O, Petković V, Petringa G, Cirrone P, Cuttone GAP. 2020. A radiobiological study of carbon ions of different linear energy transfer in resistant human malignant cell lines. Int J Radiat Biol. 96(11):1400–1412. [Taylor & Francis Online], [Web of Science ®], [Google Scholar]
55. Petrović I, Ristic-
Fira A, Todorovic D, Koricanac L, Valastro L, Cirrone P, Cuttone G. 2010. Response of a radioresistant human melanoma cell line along the proton spread-out Bragg peak . Int J Radiat Biol. 86(9):742–751. [Taylor & Francis Online], [Web of Science ®], [Google Scholar]
56. Petrović I, Ristić-
Fira A, Todorović D, Valastro L, Cirrone P, Cuttone G. 2016. Radiobiological analysis of human melanoma cells on the 62 MeV CATANA proton beam. Int J Radiat Biol. 2:215–265. [Google Scholar]
57. Ray S, Cekanaviciute E, Lima IP, Sørensen BS, Costes SV. 2018. Comparing photon and charged particle therapy using DNA damage biomarkers. Int J Part Ther. 5(1):15–24. [Crossref], [PubMed], [Google Scholar]

58. Redon CE, Dickey JS, Bonner WM, Sedelnikova OA. 2009. γ-H2AX as a biomarker of DNA damage induced by ionizing radiation in human peripheral blood lymphocytes and artificial skin. Adv Space Res. 43(8):1171–1178. [Crossref], [PubMed], [Web of Science ®], [Google Scholar]
59. Ristić
Fira A, Keta O, Petković V, Cammarata FP, Petringa G, Cirrone GAP, Cuttone G, Inc erti S, Petrović I. 2020. DNA damage assessment of human breast and lung carcinoma cells irradiated with protons and carbon ions. J Radiat Res App Sc. 13:672–687. [Web of Science ®], [Google Scholar]
60. Romano F, Cirrone GA, Cuttone G, Rosa FD, Mazzaglia SE, Petrovic I, Fira AR, Vari sano A. 2014. A Monte Carlo study for the calculation of the average linear energy transfer (LET) distributions for a clinical proton beam line and a radiobiological carbon ion beam line. Phys Med Biol. 59(12):2863–2882. [Crossref], [PubMed], [Web of Science ®], [Google Scholar]
61. Roots R, Okada S. 1972. Protection of DNA molecules of cultured mammalian cells from radiation-induced single-strand scissions by various alcohols and SH compounds. Int J Radiat Biol Relat Stud Phys Chem Med. 21(4):329–342. [Taylor & Francis Online], [Web of Science ®], [Google Scholar]
62. Rothkamm K, Horn S. 2009. Gamma-H2AX as protein biomarker for radiation exposure. Ann Ist Super Sanita. 45(3):265–271. [PubMed], [Web of Science ®], [Google Scholar]
63. Sage E, Shikazono N. 2017. Radiation-induced clustered DNA lesions: repair and mutagenesis. Free Radic Biol Med. 107:125–135. [Crossref], [PubMed], [Web of Science ®], [Google Scholar]
64. Sakata D, Belov O, Bordage MC, Emfietzoglou D, Guatelli S, Inaniwa T, Ivanchenko V, Karamitros M, Kyriakou I, Lampe N, et al. 2020. Fully integrated Monte Carlo simulation for evaluating radiation induced DNA damage and subsequent repair using Geant4-DNA. Sci Rep. 10(1):20788. [Crossref], [PubMed], [Web of Science ®], [Google Scholar]
65. Sakata D, Lampe N, Karamitros M, Kyriakou I, Belov O, Bernal MA, Bolst D, Bordage MC, Breton V, Brown JMC, et al. 2019. Evaluation of early radiation DNA damage in a fractal cell nucleus model using Geant4-DNA. Phys Med. 62:152–157. [Crossref], [PubMed], [Web of Science ®], [Google Scholar]
66. Schipler A, Iliakis G. 2013. DNA double-strand-break complexity levels and their possible contributions to the probability for error-prone processing and repair pathway choice. Nucleic Acids Res. 41(16):7589–7605. [Crossref], [PubMed], [Web of Science ®], [Google Scholar]
67. Shim G, Normil MD, Testard I, Hempel WM, Ricoul M, Sabatier L. 2016. Comparison of individual radiosensitivity to γ-rays and carbon ions. Front Oncol. 6:137. [Crossref], [PubMed], [Web of Science ®], [Google Scholar]
68. Suzuki M, Kase Y, Yamaguchi H, Kanai T, Ando K. 2000. Relative biological effectiveness for cell-killing effect on various human cell lines irradiated with heavy-ion medical accelerator in Chiba (HIMAC) carbon-ion beams. Int J Radiat Oncol Biol Phys. 48(1):241–250. [Crossref], [PubMed], [Web of Science ®], [Google Scholar]
69. Tommasino F, Durante M. 2015. Proton radiobiology. Cancers. 7(1):353–381. [Crossref], [PubMed], [Web of Science ®], [Google Scholar]

70. van de Water TA, Lomax AJ, Bijl HP, de Jong ME, Schilstra C, Hug EB, Langendijk JA. 2011. Potential benefits of scanned intensity-modulated proton therapy versus advanced photon therapy with regard to sparing of the salivary glands in oropharyngeal cancer. Int J Radiat Oncol Biol Phys. 79(4):1216–1224. [Crossref], [PubMed], [Web of Science ®], [Google Scholar]
71. Vitti ET, Parsons JL. 2019. The radiobiological effects of proton beam therapy: impact on DNA damage and repair. Cancers. 11(7):946. [Crossref], [Web of Science ®], [Google Scholar]
72. Wallace SS. 1998. Enzymatic processing of radiation-induced free radical damage in DNA. Radiat Res. 150(5 Suppl):S60–S79. [Crossref], [PubMed], [Web of Science ®], [Google Scholar]
73. Weber U, Kraft G. 2009. Comparison of carbon ions versus protons. Cancer J. 15(4):325–332. [Crossref], [PubMed], [Web of Science ®], [Google Scholar]
74. Weyrather WK, Kraft G. 2004. RBE of carbon ions: experimental data and the strategy of RBE calculation for treatment planning. Radiother Oncol. Suppl. 73:S161–S9. [Crossref], [PubMed], [Web of Science ®], [Google Scholar]
75. Zhang X, Ye C, Sun F, Wei W, Hu B, Wang J. 2016. Both complexity and location of DNA damage contribute to cellular senescence induced by ionizing radiation. PLOS One. 11(5):e0155725. [Crossref], [PubMed], [Web of Science ®], [Google Scholar]
76. Zlobinskaya O, Dollinger G, Michalski D, Hable V, Greubel C, Du G, Multhoff G, Röp er B, Molls M, Schmid TE. 2012. Induction and repair of DNA double-strand breaks assessed by gamma-H2AX foci after irradiation with pulsed or continuous proton beams. Radiat Environ Biophys. 51(1):23–32. [Crossref], [PubMed], [Web of Science ®], [Google Scholar]

- **Education**
- **Engineering & Technology**
- **Environment & Agriculture**
- **Environment and Sustainability**
- **Food Science & Technology**
- **Geography**
- **Global Development**
- **Health and Social Care**
- **Humanities**
- **Information Science**
- **Language & Literature**
- **Law**
- **Mathematics & Statistics**
- **Medicine, Dentistry, Nursing & Allied Health**
- **Museum and Heritage Studies**
- **Physical Sciences**
- **Politics & International Relations**
- **Social Sciences**
- **Sports and Leisure**
- **Tourism, Hospitality and Events**
- **Urban Studies**

Information for

- Authors
- Corporate partners
- Editors
- Librarians
- Societies

Open access

- Overview
- Open journals
- Open Select
- Dove Medical Press
- F1000Research

Opportunities

- Reprints and e-prints
- Advertising solutions

- Accelerated publication
- Corporate access solutions

Help and information

- Help and contact
- Newsroom
- All journals
- Books

Keep up to date

Register to receive personalised research and resources by email
Sign me up

Taylor and Francis Group Facebook page

Taylor and Francis Group Twitter page

Taylor and Francis Group Linkedin page

Taylor and Francis Group Youtube page

Taylor and Francis Group Weibo page

Registered in England & Wales No. 3099067
5 Howick Place | London | SW1P 1WG

Taylor & Francis Group
an **informa** business